The International Journal of Advanced Manufacturing Technology (2024) 135:4975–4987
https://doi.org/10.1007/s00170-024-14797-w

ORIGINAL ARTICLE

Analysis of the relationship between cutting forces and local structural properties of Scots pine wood aided by computed tomography

Yunbo Huang[1] · Daniel Chuchala[2,4] · Dietrich Buck[1] · Kazimierz A. Orlowski[2] · Magnus Fredriksson[1] · Mikael Svensson[1,3]

Received: 15 July 2024 / Accepted: 4 November 2024 / Published online: 14 November 2024

Abstract
X-ray computed tomography (CT) is utilised in some sawmills today, primarily for enhancing value yield and for process automation, which includes log sorting and sawing optimisation. Nevertheless, there is a scarcity of recent research utilising CT to assess the local cutting process. As a preliminary study, this paper addresses this gap by using CT to investigate the connections between local cutting force and local wood properties including density, knots, and annual ring width. Workpieces of Scots pine (*Pinus sylvestris* L.), from Sweden and Poland, were CT-scanned in laboratory conditions. Quasi-linear cutting tests were then performed on both clear and knotty regions of the workpieces using a custom-made laboratory stand with a Stellite-tipped tooth mounted on piezoelectric sensors. It was found that density influences cutting forces for both clear and knotty wood, and this effect increased noticeably with increasing uncut chip thickness. Changes in wood density, such as between sapwood and heartwood or between clear wood and knot, caused dynamic changes in cutting forces and temporary disturbances to the stability of the system. Normalisation of cutting forces by local density allowed the conclusion that density is not the only property affecting cutting forces. Other structural properties, e.g. annual ring width and latewood–earlywood proportion may affect the cutting process as well, which requires deeper analysis in the future research. This preliminary study demonstrates the feasibility and usefulness of coupling CT data with cutting force measurements and suggests further research on the relationship between cutting force and wood properties.

Keywords Computed tomography · Knots · Local wood density · Machining · Material processing · Normalisation by density · Sawing

1 Introduction

Wood is a material obtained by processing harvested or naturally fallen trees, and it has been used for thousands of years [1]. Developments in wood processing technology, including new, more efficient methods of drying, impregnating, and modifying wood, as well as the emergence of new solutions, such as glued laminated timber (GLT) and cross-laminated timber (CLT), have allowed wood to be used more suitably with regard to mechanical and physical properties [2, 3].

✉ Daniel Chuchala
daniel.chuchala@pg.edu.pl

Yunbo Huang
yunbo.huang@ltu.se

Dietrich Buck
dietrich.buck@ltu.se

Kazimierz A. Orlowski
kazimierz.orlowski@pg.edu.pl

Magnus Fredriksson
magnus.1.fredriksson@ltu.se

Mikael Svensson
mikael.svensson@lsab.se

[1] Wood Science and Engineering, Luleå University of Technology, Skellefteå, Sweden

[2] Faculty of Mechanical Engineering and Ship Technology and EkoTech Center, Institute of Manufacturing and Materials Technology, Gdańsk University of Technology, Gdańsk, Poland

[3] LSAB, Research and Development, Svinöhed 415, 77673 Långshyttan, Sweden

[4] Sylva Sp. z o.o., Wiele, Poland

Modern wood processing technologies, to ensure efficient and sustainable use of material, require adequate knowledge of the raw materials, i.e. wood logs, before processing. Based on information including shape, dimensions, and internal structure of the material, logs are sorted for different processing routes and final products. Log sorting methods and strategies have a distinct impact on whether the wood can be put to maximum beneficial use with minimal material waste for the production of suitable products [4].

Currently, X-ray computed tomography (CT) scanning provides the highest value-yield results for sorting wood by assessing its internal structure. This method is based on the process of transmitting X-rays into the wood log and subsequently measuring the X-ray attenuation on the opposite side. With CT, the internal structure of wood can be reconstructed by integrating projections obtained from various angles around the log axis [5]. The spatial reconstruction of CT scanning data plays a vital role in identifying internal log features, including knot positions [6–8], fibre orientation [9], annual ring width [10], and the density of the wood [11]. Identification and validation of these structural properties of wood allow the production of high-quality wood products with the highest possible market value. This is primarily because the mechanical and physical properties of wood products are distinctly affected by all of these structural properties, especially wood density [12, 13], knots [14, 15], and fibre direction [16, 17]. The same structural properties of wood affect machinability properties, such as cutting forces and cutting power.

A limited number of initial studies examined local wood properties, comparing density and cutting forces, at a knot [18], in both frozen and non-frozen workpieces [19], as well as for different fibre orientations [20]. The pioneering CT scans for these historic cutting experiments were conducted at Skellefteå Hospital, as documented by Lundberg in 1994 [21]. More recently, Chuchala et al. [22] analysed the effect of density on cutting forces, providing a contemporary perspective on this research. Based on the results of Chuchala et al. [22], the following studies examined cutting power and/or cutting forces normalised by wood density [23–26]. However, only the global wood density was used in the aforementioned studies, the local wood density was not accessible. The effect of wood knots on cutting forces was analysed by Caceres et al. [27] and showed a distinct impact of knots on cutting forces, which was related to the higher density of knots compared to clear wood. A similar effect of knots on cutting power was observed by Licow et al. [24]. As for the directionality of wood fibres, and its effect on machinability properties, this has been demonstrated in the work of Kivimaa [28], among others, and more recently by Moradpour et al. [29], Pinkowski et al. [30], Zhu et al. [31], and Curti et al. [32]. The main factors affecting the cutting forces are the cutting parameters and the type of cutting process, as shown, among other things, in the works of Cristóvão et al. [33], Hernandez et al. [34], Zhu et al. [35], Nasir and Cool [36], and Pantscharowitsch and Kromoser [37].

Currently, CT scanners used in some state-of-the-art sawmills allow log movement speeds of up to 180 m/min (MiCROTEC) and offer extensive information about the internal structure of the scanned log. This data is used to optimise log sawing patterns and properly the log to obtain higher-value sawn products. These advancements are the result of numerous studies, including those by Berglund et al. [38] and Fredriksson [39–41]. However, high-speed CT scanners have not yet been widely used in the industry. This research takes the next step in utilising CT scanning for sawing and cutting process optimisation in sawmills.

The objective of this present study was to determine the feasibility of coupling cutting behaviour and local properties of Scots pine as revealed by CT imaging. Specifically, at this stage, cutting behaviour was addressed solely by the magnitude of the cutting force in the primary direction, and only material properties that are directly associated with density were considered, including knots. In the literature available to date, no analysis of the relationship between cutting forces and local wood density determined using computed tomography has been carried out.

2 Materials, methods, and data processing

2.1 Materials

Six Scots pine (*Pinus sylvestris* L.) specimens were collected, three from northern Sweden by Sävar sawmill, and three from northern Poland by Sylva Sp. z o.o. Specimens were prepared in a square cross section, and each specimen was obtained from a different log. The three specimens from Sweden measured 75 mm × 75 mm × 2500 mm in width, height, and length, respectively; the three specimens from Poland measured 70 mm × 70 mm × 2000 mm in width, height, and length, respectively. Specimens were chosen to include substantial structural differences, such as clear wood, different groups of knots within one specimen, and various annual ring widths across specimens. After being kiln-dried in industry conditions, the specimens were stored in a climatic chamber at a temperature of $T = 20$ °C and a relative humidity of $RH = 65\%$, which corresponds to an equilibrium moisture content of $MC = 12\%$.

The specimens underwent scanning using a laboratory CT scanner Mito (MiCROTEC, Bressanone, Italy) after the desired *MC* of 12% was reached. The scanning resolution was 0.3 mm in all three directions, i.e. employing 0.3-mm voxels. CT data were imported to 3D Slicer, version 5.0.3 (The Slicer Community, Boston, MA, USA), which was used to visually assess knot locations inside the specimens.

Based on the visual inspection in 3D Slicer, a segment of approximately 250 mm in length was chosen from each of the six specimens to ensure that one end of the cross section contained only clear wood (Fig. 1), while the other end of the cross section contained knotty wood (Fig. 2). These 250-mm specimens are hereafter referred to as the workpieces.

2.2 Cutting machine, cutting parameters, and cutting tools

Figure 3 depicts the test machine setup that measures the forces exerted during the process of cutting wooden workpieces using a solitary tooth. Previous cutting force measurements have been performed on this machine [42–44]. It should be emphasised that for this kinematic system, the relative motion of the tool to the workpiece is quasi-linear.

The testing machine consists of three main parts: the frame, safety grid, and drivetrain; the rotating arm that holds the workpiece; and the platform that includes the measuring block and sliding rails in both feeding and side directions. The wood workpiece is securely affixed to the rotating arm using four bolts. The arm, with a radius of 540 mm including the clamped workpiece, undergoes clockwise rotation at a speed of 276 revolutions per minute, leading to a linear speed of $v_c = 15.6\ \mathrm{m \cdot s^{-1}}$.

Three piezoelectric sensors are connected to the tooth holder, each aligned with one of the three orthogonal directions, namely, the primary, side, and feeding directions. These sensors are used to quantify the force components exerted on the tooth throughout the cutting procedure. The cutting tooth (Fig. 3a and b) is fixed in place by the tooth holder, and feeding movement is provided by a stepper motor and guided by the sliding rails.

Measurement of the cutting force in the primary direction involved calculating the moment exerted on the three sensors. This moment was a result of the eccentricity between the tooth tip and the centre of the sensor in the primary direction, as well as any potential misalignment.

The tip of the tooth was loaded statically with a known weight of 500 g in three orthogonal directions. A calibration matrix was therefore derived based on the sensor readings and the known weight and was used to convert measured amplitudes in the three sensors into cutting force in the main direction. The same principle was applied to cutting force

Fig. 1 Cross sections of the clear wood. Three grooves were cut on each of the six cross sections. Cutting direction was left to right, as shown in the picture. The markings on the cross sections are only for identifying the workpieces during the experiments. t0, t1, t2, t3, t4, and t5 are numbers of analysed samples

Fig. 2 Cross section of the knotty wood side. Three grooves were cut on each of the six cross sections. Cutting direction was left to right, as shown in the picture. The markings on the cross sections are only for identifying the workpieces during the experiments. t0, t1, t2, t3, t4, and t5 are numbers of analysed samples

in other directions, although they are not discussed in this paper.

Details of the cutting tooth are as follows: the tooth was tipped with Stellite™ 12 (Deloro Wear Solutions GmbH, Koblenz, Germany), side clearance angle $\alpha_f = 12°$, side rake angle $\gamma_f = 27°$, overall set (theoretical kerf) $S_t = 2.87$ mm and saw blade thickness $s = 1.47$ mm (Fig. 3c). After sharpening, the main cutting edge was rounded to a radius of about $r_o = 20$ µm. This is the same cutting tooth geometry that is currently applied in numerous Swedish sawmills [43, 44]. The single tooth was obtained by cutting it off from a typical band saw blade.

Three grooves were planned on each knotty side to cross as large an area of knots as possible, with feed per arm revolution being 0.3 mm, 0.5 mm, and 0.7 mm, respectively. Three grooves were made on the clear wood side, at positions corresponding to the grooves on the knotty side, with feed per arm revolution being 0.5 mm, 0.7 mm, and 1.1 mm, respectively. Due to the fine spatial detail level, CT data can be seen as a digital "twin" of the real wood. Therefore, in the 3D data, it is possible to locate the regions being cut, as well as the local wood features that the cutting tooth encounters. Fifteen cuts were made for each groove. From the point of view of the cutting process, the theoretical feed per revolution is equal to the uncut chip thickness h.

Because of the testing machine setup, the tooth cut the wood workpieces in a quasi-linear manner, i.e. circular cutting with a large rotation radius, referred to as the arc path (Fig. 4). Consequently, during the initial series of incisions, the two corners of the workpiece were excised, while the central portion remained unaltered. Force readings from the first five cuts were therefore excluded, as the initial cutting process was not complete along the path.

2.3 Measuring and collecting data

The flow of the entire experiment and the data collection process used for the analysis are shown in Fig. 4. The natural frequencies of the measuring block were determined by striking the tooth with a steel hammer in three orthogonal directions. These were measured to be 4.4 kHz, 2.5 kHz, and 2.5 kHz in the primary cutting, feeding, and side directions, respectively. Analog signals from the three sensors were amplified using three type 2635 charge amplifiers (Brüel

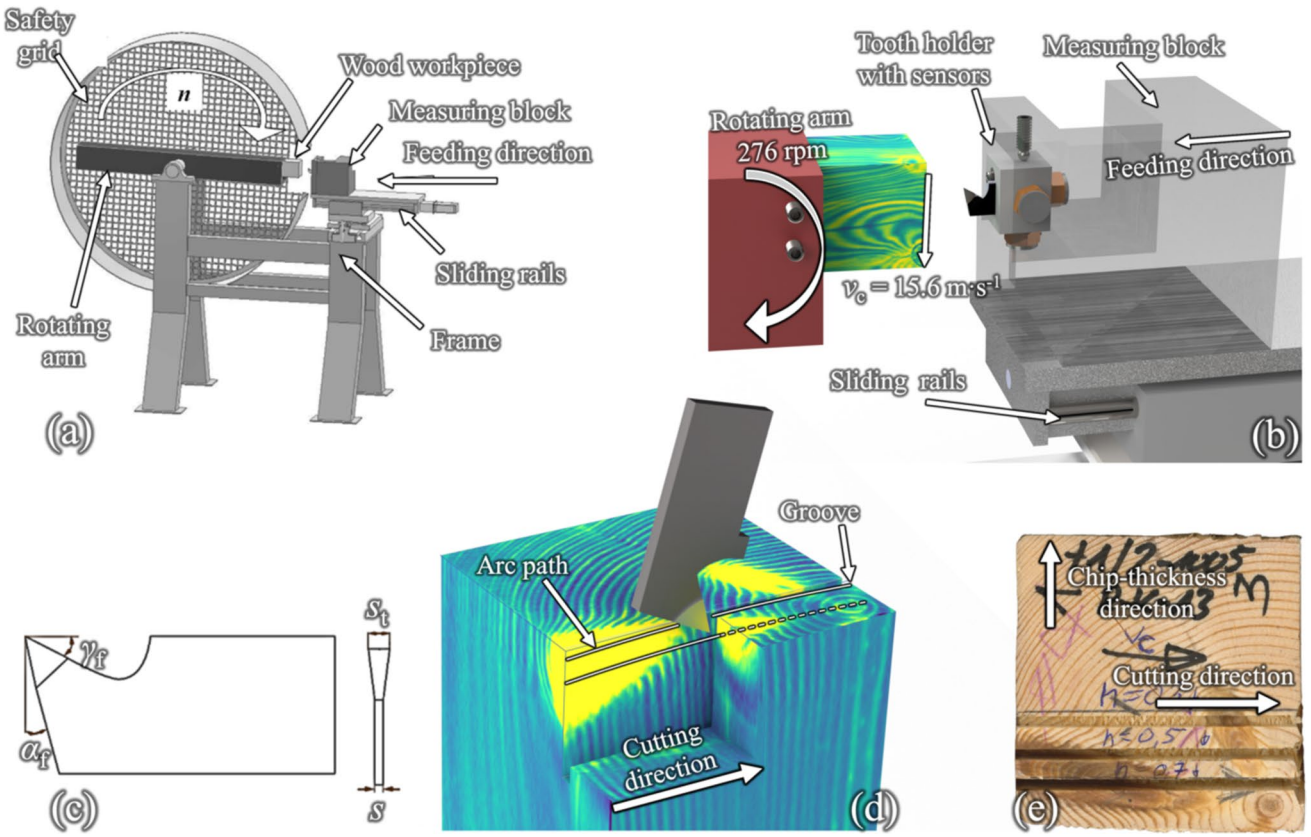

Fig. 3 Cutting station implementing quasi-linear cutting process: general view (**a**), detailed view of cutting zone (**b**), cutting tooth geometry (**c**), three-dimensional representation of the workpiece from CT data (**d**), and the scanned cross section (**e**). Note that images **d** and **e** represent the same workpiece as in Fig. 6

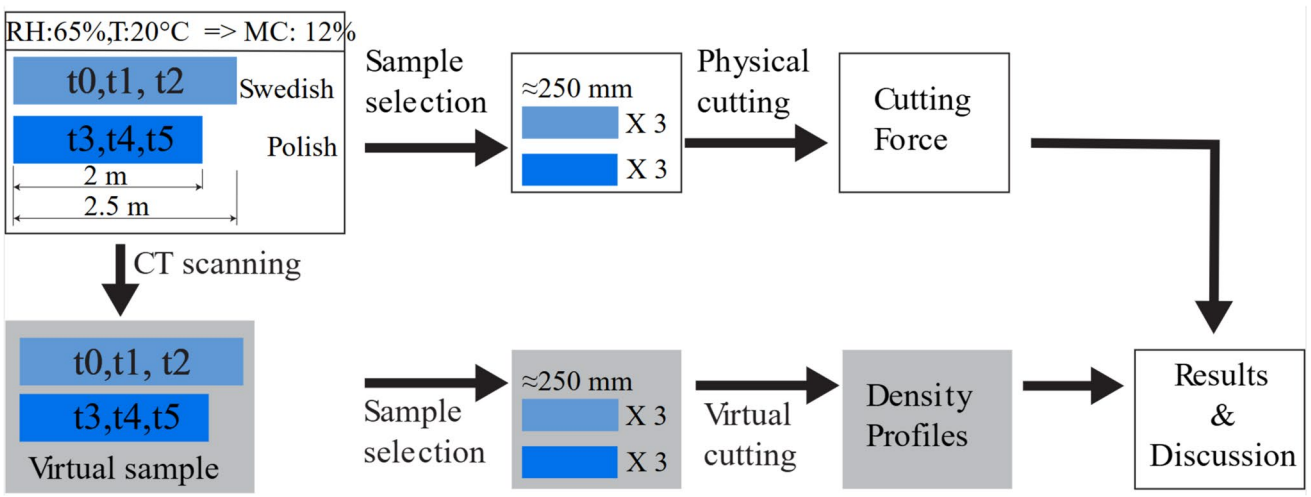

Fig. 4 Experimental flow and data collection process. t0, t1, t2, t3, t4, and t5 are numbers of analysed samples; RH, relative humidity; MC, moisture content

& Kjær, Denmark) and then sampled at 60 kHz using a PCI-6023E0 data acquisition card in LabVIEW 2013 software (National Instruments, USA). The digitised signals were then subjected to a Butterworth filter to eliminate frequency components exceeding 800 Hz. Following this, the data was converted into forces using the calibration matrix.

The mean cutting force from the last ten cuts of each groove was obtained as a 1D array, referred to as the cutting force profile. At a sampling rate of 60 kHz and a cutting speed of 15.6 $m \cdot s^{-1}$, each sampling point corresponds to a distance of 0.262 mm.

Groove positions were measured on the workpieces after the cutting tests and used to locate the groove positions on the three-dimensional CT density models, as actual cut grooves may deviate slightly from the planned ones. Voxels corresponding to the chips removed during the cutting process were extracted from the CT data as 3D arrays. Mean density across the chip-thickness direction (Fig. 3e) was then obtained as a 2D array; Fig. 5 shows examples of rendered images of these 2D arrays. The mean density for the chips removed during the last ten cuts was obtained as a 1D array, referred to as the density profile. As one voxel represents a known distance of 0.3 mm, the cutting force profile was then adjusted to match the scale of CT images and density profiles when plotting the results, as exemplified in Fig. 5.

2.4 Statistical analysis

An analysis of variance (ANOVA) was performed on the measured cutting force and was used to determine the significance of differences between cutting forces measured for pine wood with three different values of uncut chip thickness [45]. This statistical analysis was conducted at the assumed significance level $\alpha = 0.05$.

3 Results and discussion

Twelve cases were examined across the six wood workpieces, i.e. one knotty side and one clear side for each workpiece, and a detailed analysis is presented for four of these cases. The four cases presented demonstrate the impact of knot orientation, annual ring width, and wood type on cutting forces and—a key focus of this research—on density. The remaining eight cases fall into the categories represented by the four presented cases. The influence of system stiffness on measured cutting force is also discussed.

It should be borne in mind, however, that this is only an indicative study intended to determine the existence of possible relations between cutting force and local wood properties. No statistically supported conclusions regarding the correlation between cutting force and local wood properties can be drawn based on the presented results.

Local cutting force trended upward with increasing uncut chip thickness. However, this force also exhibited distinct variations attributed to the specific properties of the wood material the tooth encountered. Subsequent subsections delve into a more detailed analysis of the variations in cutting force.

3.1 Case 1: density/annual ring width

Figure 5 demonstrates how the cutting force is related to local wood density: lower density resulted in lower cutting force; higher density resulted in higher cutting force. The three grooves were radially incised, and the density profile exhibited a slight increase towards the end of the incision. The observed increase might be attributed to the narrower annual rings.

This observation may derive from the fact that juvenile wood is distinguished by widely spaced annual rings, whereas mature wood exhibits closely compacted annual rings. Juvenile wood exhibits reduced strength compared to mature wood, and the two wood types differ in microfibril angle magnitude, cell length, and density [46] of the S2 microfibril layer.

Chuchala et al. [26] noted an increase in cutting forces for increased wood density, which is largely dependent on the proportion of latewood in the annual growth. Latewood has more than twice the density of earlywood and significantly affects the mechanical properties of the wood [47]. Chuchala et al. [26] proposed that analyses normalise the cutting force by wood density and even by latewood–earlywood ratio.

Wood density can be determined with high accuracy using the CT scanner; however, determining latewood–earlywood ratio under industry conditions by CT scanner is difficult [48, 49]. Therefore, it seems practical to normalise the local cutting forces by the local density, as shown in Fig. 5c. Normalising cutting forces by density reduced the peaks of the cutting force profile in areas with narrow annual rings. This is particularly noticeable for the smaller uncut chip thickness $h_0 = 0.5$ mm, confirming the observation of Chuchala et al. [22] that the effect of density on cutting forces becomes more noticeable with increasing uncut chip thickness.

It was also observed that the cutting force is more sensitive to changes in the local density as the uncut chip thickness increases. Similar relations were reported by Chuchala et al. [22]; however, in that study, the differences in uncut chip thickness values were relatively greater and the analysed wood originated from a different geographic location than that in this study.

A close relation between local density and cutting forces was also observed for knotty wood. Knots have more than twice the density of clear wood, and these differences were also reflected in the cutting force profile (Fig. 6). Similar observations were presented by Caceres et al. [27] when analysing the peripheral orthogonal milling processes of spruce wood. They also distinguished separate zones before and after the knot, which showed differences in the structure of the wood and, consequently, in the cutting force values. A noticeable variation in cutting power during the sawing process of pine wood with

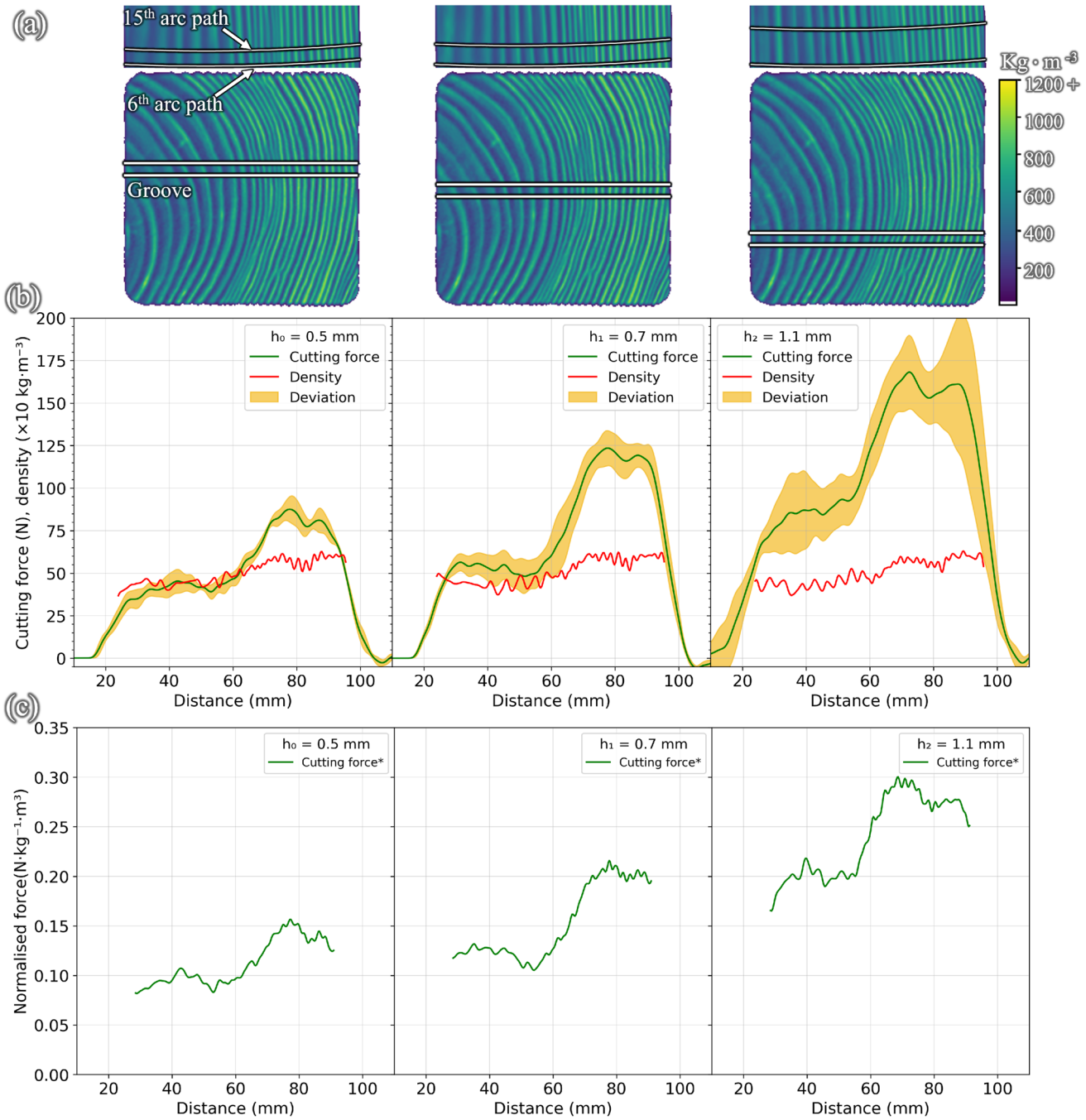

Fig. 5 Cutting force and density profile when cutting clear wood: X-ray computed tomography (CT) image of the clear wood (**a**), cutting force and density profile (**b**), cutting force normalised by density (**c**). Asterisk (*) denotes the cutting force that is normalised by wood local density. For each uncut chip thickness, the corresponding CT images in **a** cutting force and density profiles in **b** and the normalised cutting force profile in **c** are aligned vertically

knots was also observed and analysed by Licow et al. [24]. However, compared to the measurement of cutting forces, the measurement of cutting power is less sensitive to changes in wood structure in the form of annual ring width variations.

3.2 Case 2: knot orientation/knot type

A knot can be viewed as a miniature tree with its own pith and orientation. Knot orientation in relation to cutting direction was observed to affect the cutting force. For the smallest

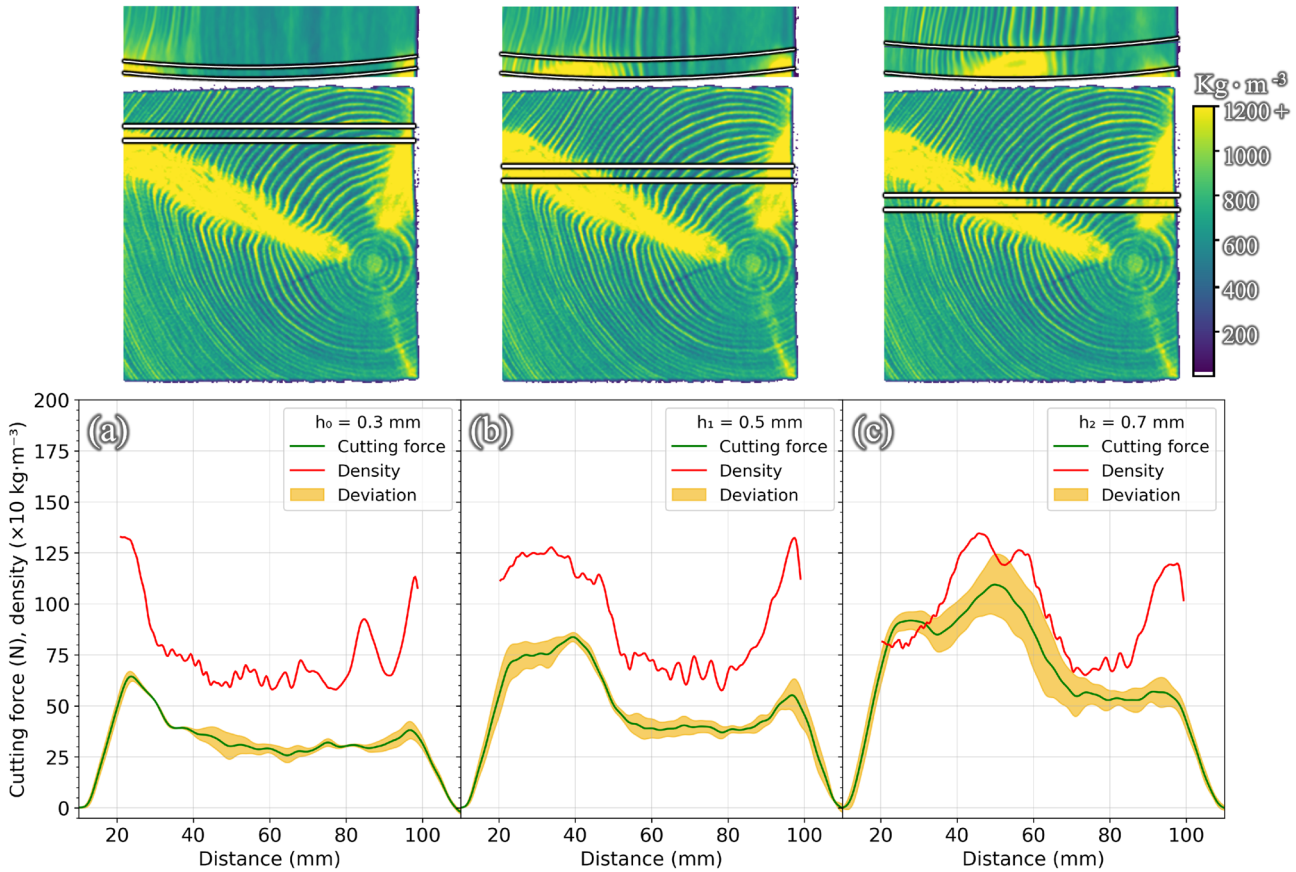

Fig. 6 Cutting force and density profile when cutting knot in the transverse direction

uncut chip thickness of $h_0 = 0.3$ mm, in Fig. 6, cutting force followed the trend of density profile. For the larger uncut chip thicknesses, i.e. 0.5 mm and 0.7 mm, the cutting force did not follow the same density profile as for 0.3 mm. In particular, at the larger, leftmost knot, density was steadily high while cutting force rose gradually. This phenomenon could be explained by the effect of knot orientation on cutting force. The smaller knot was sawn in a more cross-cut manner, which means that the cutting direction was perpendicular to the annual rings and fibres of the knot. By contrast, the larger knot was sawn in a more rip-cut manner, which means that the cutting direction was parallel to or along with the wood fibres. Cross-cutting generally requires more force than rip-cutting. Therefore, the orientation of knots affected how much force was needed to cut through them.

Figure 7 also shows that for both $h_1 = 0.5$ mm and $h_2 = 0.7$ mm, the cutting force peaked at transition regions between knot and clear wood. These regions were characterised by sudden changes in fibre direction from parallel to orthogonal relative to the cutting direction. These changes created more resistance to cutting than did regions with uniform fibre orientation inside the knot. The sharp decrease in cutting force after these regions corresponded to a decrease in density.

The density profile for $h_1 = 0.5$ mm and $h_2 = 0.7$ mm were similar to each other over almost the entire cutting length, but the cutting force profiles were noticeably different. Cutting force for $h_2 = 0.7$ mm is not always higher than for $h_1 = 0.5$ mm at the knot regions in Fig. 7. This indicates that cutting force is a result of multi-factor interactions; analyses of any single factor cannot sufficiently depict the cutting behaviour.

Figure 6 provides a contrasting example to Fig. 7. In Fig. 6, both knots were cut at comparable angles within three grooves. The observed outcome was a consistent pattern in the behaviour of the cutting force, whereby an increase in density at both knots resulted in a corresponding increase in cutting force. The knot in Fig. 8 was cut in a similar way as for the knot in Fig. 7. However, Fig. 8 also shows how this type of knot affects the course of the cutting forces. Cutting forces generated in the dead part of the knot were noticeably lower compared to cutting forces generated in the sound part of the knot. The dead knot is reflected as two slight drops in the density profile (Fig. 8b). An alternate visualisation of this knot is shown in Fig. 2, workpiece t5.

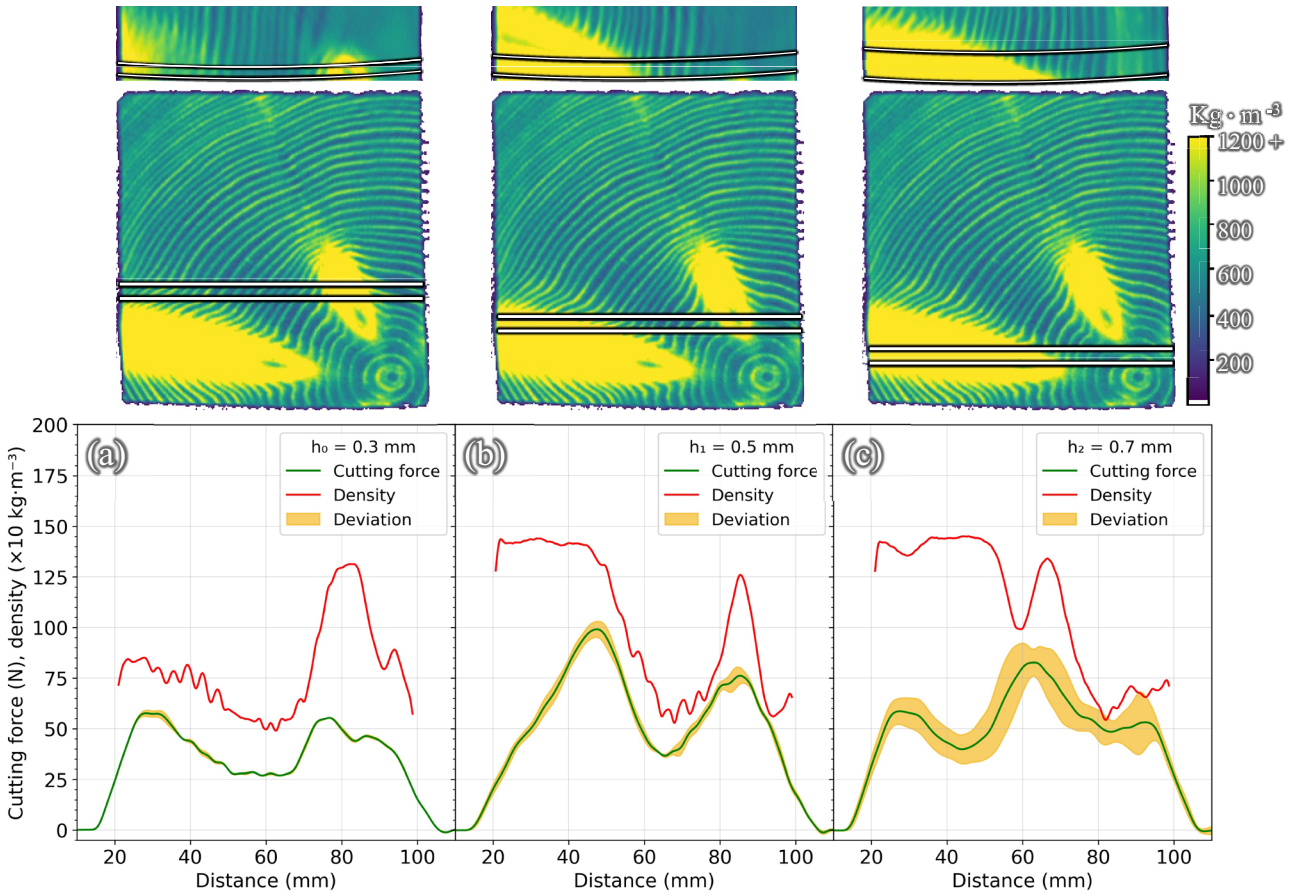

Fig. 7 Cutting force and density profile when cutting knot in the longitudinal direction

3.3 Case 3: system stability

The system was observed to lose stability when the cutting blade entered and exited the wood workpiece (Fig. 9). This phenomenon was also noticed when the cutting blade entered transition zones, i.e. from regions of lower density (heartwood and/or juvenile wood) to regions of higher density (sapwood and/or knots). This loss of stability manifests itself through a sharp peak or fall in the cutting forces above/below the otherwise normal level for the cutting forces of the material of a given density, and it is caused by dynamic processes analogous to interrupted machining of isotropic materials, such as metals [50, 51]. Upon entering the harder material, cutting forces increase rapidly, recorded as a peak in the force waveform. This produces vibration, and the system needs time to stabilise. However, before stabilisation of the cutting process is achieved, the blade exits the material, which is another destabilising factor (Fig. 9).

When cutting knots at the very beginning and the very end of the cutting process, lower cutting forces were recorded. This was probably due to the aforementioned disruption of stability. However, when cutting longer knot areas, the course of the cutting forces was stable (Fig. 8c).

A similar phenomenon of loss of stability of the system was observed during tests of quasi-linear cutting of beech wood with high cutting speeds of up to 80 $m \cdot s^{-1}$, the results of which were presented in the papers by Dvoracek et al. [52] and Kubik et al. [53]. Losses of stability also occurred at the entry and exit of the cutting blade from the material being cut. These phenomena are difficult to eliminate from the cutting process on systems with low stiffness like the one used in this study. Removing these artefacts from the measurements would require a great deal of the processing of the raw data through appropriate filtering of relevant frequency bands.

Based on the analysed results, it can be concluded that cutting forces depend on the density of machined wood. However, this relationship increases as the uncut chip thickness increases (Fig. 5c). Normalising the cutting force by the density of the machined material allows elimination of the effect of density on cutting force during analysis [23–26]. Figure 10 shows the dependence of density-normalised cutting forces on the uncut chip thickness. Despite eliminating

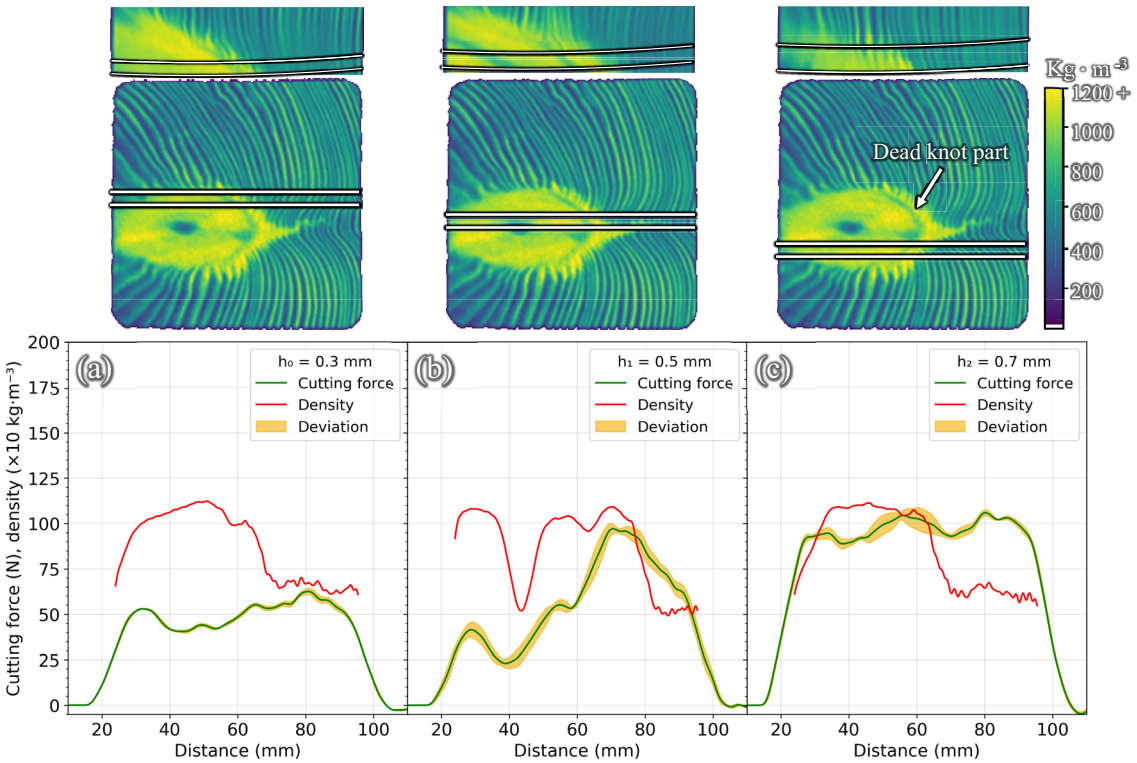

Fig. 8 Cutting force and density profile when cutting through a dead knot

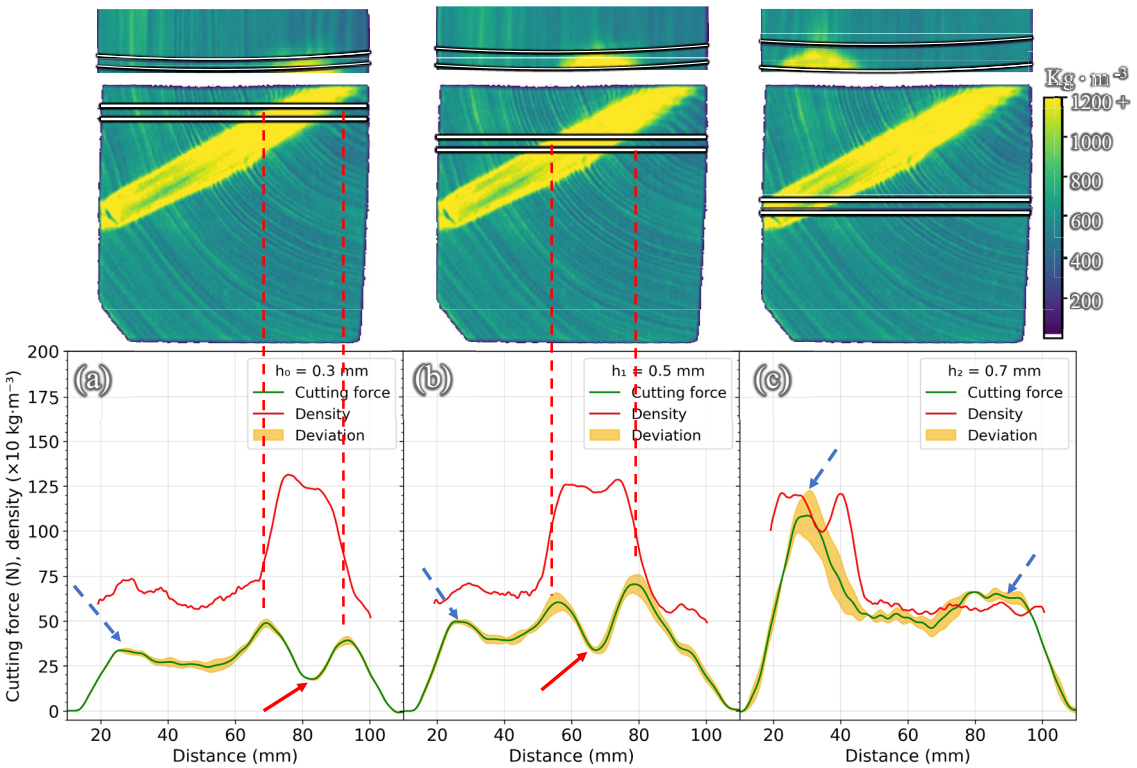

Fig. 9 Unstable course of cutting forces during the cutting of knotty pine wood

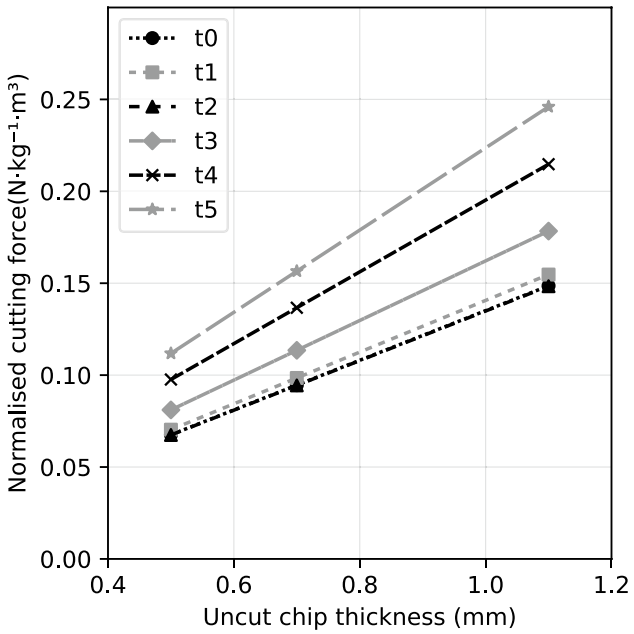

Fig. 10 Density-normalised mean cutting forces as a function of uncut chip thickness for the six analysed clear wood workpieces t0, t1, t2, t3, t4, and t5

the effect of density on the cutting forces, there are still statistically significant differences between workpieces in regard to cutting force for each of the analysed uncut chip thicknesses (for h_0 the probability was $p = 7.5 \cdot 10^{-18}$; h_1: $p = 2.2 \cdot 10^{-19}$; h_2: $p = 5.5 \cdot 10^{-14}$).

The observed differences in normalised cutting force may be due to differences in other structural parameters of the machined material, such as the width of the annual rings, the proportion of latewood to earlywood, fibre direction, and the annual ring radius in the cutting area. Such differences were present in the workpieces analysed (Fig. 1). Moreover, it was also observed that in the case of very small and constant widths of annual rings (Fig. 1: t0, t1, and t2), the cutting properties of wood are more similar to those of isotropic material. The density of the cut wood is then one of the most important factors influencing the cutting forces, therefore the normalisation of the cutting forces by the local density leads to no differences between the cutting forces for the analysed samples. Such a phenomenon was observed for samples t0, t1, and t2 (Fig. 10), with lower values for the thickness of the uncut chip (for h_0 the probability was $p = 0.33$; h_1: $p = 0.54$). The above observations provide directions for further research into the effectual use of CT images for the design and development of the wood-cutting process.

However, the presented results suggest that when investigating the wood-cutting process and, for example, analysing the effect of cutting parameters on cutting force and/or cutting power or similar, normalisation of these cutting forces and cutting powers by local density should be carried out. Since the variability of wood density is significant and its influence on cutting forces is noticeable, in the absence of this normalization the analysis of the machinability will be disturbed by the influence of density differences in the analysed samples.

4 Conclusions

This study's objective was to determine the viability of utilising X-ray computed tomography (CT) data to establish relationships between specific wood properties and cutting behaviour. Variations in wood workpieces were deliberately incorporated to replicate realistic scenarios, encompassing clear wood, knots, and workpieces with varying annual growth ring distances. The following conclusions can be drawn based on the results:

1. CT images reveal the wood local density and details of the knots inside the wood, which makes possible a more accurate analysis of the wood-cutting process.
2. Cutting force is dependent on wood density; however, density is only one of the important structural properties that affect cutting force meaning that further research is needed to analyse the effect of other properties.
3. Uncut chip thickness has an important impact on cutting force, and the effect of density on cutting force becomes more noticeable as uncut chip thickness increases.
4. Loss of stability of the system introduces measurement noise for both clear and knotty wood, although the impact is more noticeable for knotty wood; this is analogous to interrupted machining.
5. Recommended further research directions: effect of knot cutting direction, annual ring width, latewood–earlywood proportion on cutting force values and their stability.

Acknowledgements The authors express their sincere gratitude for the substantial support provided by CT WOOD, a centre of excellence at Luleå University of Technology, in the advancement of X-ray computed tomography applications for the forest products industry. The authors gratefully acknowledge the financial support received from the Gdańsk University of Technology through the DEC-1/2022/IDUB/II.2/Np grant under the Neptunium Enhancing Baltic Region Research Cooperation through "The Excellence Initiative – Research University" programme. Additionally, the successful execution of this project was made feasible due to the financial support provided by the Kempe Foundation. The authors would like to express their sincere gratitude to Axel Östman from Sävar Sawmill, Sweden, and Piotr Taube from Sylva Sp. z o.o., Poland.

Author contribution Yunbo Huang: methodology, investigation, formal analysis, writing—original draft, writing—original draft, writing—review and editing, visualization.

Daniel Chuchala: conceptualization, methodology, investigation, resources, formal analysis, writing—original draft, writing—review and editing, project administration, funding acquisition.

Dietrich Buck: methodology, investigation, writing—review and editing.

Kazimierz A. Orlowski: conceptualization, methodology, investigation, writing—review and editing.

Magnus Fredriksson: methodology, investigation, writing—review and editing, funding acquisition.

Mikael Svensson: conceptualization, methodology, investigation, writing—review and editing, funding acquisition.

Funding This work was supported by CT WOOD, a centre of excellence at Luleå University of Technology, in the advancement of X-ray computed tomography applications for the forest products industry and by the Kempe Foundation.

This work was also supported by DEC-1/2022/IDUB/II.2/Np grant under the Neptunium Enhancing Baltic Region Research Cooperation through "The Excellence Initiative – Research University" programme, Gdańsk University of Technology.

Declarations

Competing interests The authors declare no competing interests.

References

1. Dani AH, Lorenzo JL, Nunoo RB, De Laet SJ (eds) (1994) History of humanity: prehistory and the beginnings of civilization. UNESCO and Routledge, New York
2. Asdrubali F, Ferracuti B, Lombardi L, Guattari C, Evangelisti L, Grazieschi G (2017) A review of structural, thermo-physical, acoustical, and environmental properties of wooden materials for building applications. Build Environ 114:307–332. https://doi.org/10.1016/j.buildenv.2016.12.033
3. Brandner R, Flatscher G, Ringhofer A, Schickhofer G, Thiel A (2016) Cross laminated timber (CLT): overview and development. Eur J Wood Wood Prod 74:331–351. https://doi.org/10.1007/s00107-015-0999-5
4. Taube P, Orlowski KA, Chuchala D, Sandak J (2020) The effect of log sorting strategy on the forecasted lumber value after sawing pine wood. Acta Facultatis Xylologiae Zvolen 62:89–102. https://doi.org/10.17423/afx.2020.62.1.08
5. Radon J (2005) Über die bestimmung von funktionen durch ihre integralwerte längs gewisser mannigfaltigkeiten. Class Papers Modern Diagn Radiol 5(21):124
6. Breinig L, Berglund A, Grönlund A, Brüchert F, Sauter UH (2013) Effect of knot detection errors when using a computed tomography log scanner for sawing control. For Prod J 63(7–8):263–274. https://doi.org/10.13073/FPJ-D-13-00068
7. Fredriksson M, Cool J, Avramidis S (2019) Automatic knot detection in coarse-resolution cone-beam computed tomography images of softwood logs. For Prod J 69(3):185–187. https://doi.org/10.13073/FPJ-D-19-00008
8. Longuetaud F, Mothe F, Kerautret B, Krähenbühl A, Hory L, Leban JM, Debled-Rennesson I (2012) Automatic knot detection and measurements from X-ray CT images of wood: a review and validation of an improved algorithm on softwood samples. Comput Electron Agric 85:77–89. https://doi.org/10.1016/j.compag.2012.03.013
9. Sepúlveda P, Kline E, Oja J (2003) Prediction of fiber orientation in Norway spruce logs using an X-ray log scanner: a preliminary study. Wood Fiber Sci 35(3):421–428
10. Onoe M, Tsao W, Yamada H, Nakamura H, Kogure J, Kawamura H, Yoshimatsu M (1984) Computed tomography for measuring the annual rings of a live tree. Nucl Instrum Methods Phys Res 221(1):213–220
11. Wang Q, Liu X, Yang S, Jiang M, Cao J (2019) Non-destructive detection of density and moisture content of heartwood and sapwood based on X-ray computed tomography (X-CT) technology. Eur J Wood Prod 77:1053–1062. https://doi.org/10.1007/s00107-019-01459-y
12. Machado JS, Louzada JL, Santos AJA, Nunes L, Anjos O, Rodrigues J, Simões RMS, Pereira H (2014) Variation of wood density and mechanical properties of blackwood (*Acacia melanoxylon* R. Br.). Mater Des 56:975–980. https://doi.org/10.1016/j.matdes.2013.12.016
13. Miyoshi Y, Kojiro K, Furuta Y (2018) Effects of density and anatomical feature on mechanical properties of various wood species in lateral tension. J Wood Sci 64:509–514. https://doi.org/10.1007/s10086-018-1730-z
14. Cherry R, Karunasena W, Manalo A (2022) Mechanical properties of low-stiffness out-of-grade hybrid pine—effects of knots, resin and pith. Forests 13(6):927. https://doi.org/10.3390/f13060927
15. Koman S, Feher S, Abraham J, Taschner R (2013) Effect of knots on the bending strength and the modulus of elasticity of wood. Wood Research 58(4):617–626
16. Jingcheng S, Zhao R, Zhong Y, Chen Y (2022) Compressive mechanical properties of larch wood in different grain orientations. Polymers 14(18):3771. https://doi.org/10.3390/polym14183771
17. Shumeng P, Liang Y, Tao W, Liu Y, Huan S, Qin H (2019) Effect of the strain rate and fiber direction on the dynamic mechanical properties of beech wood. Forests 10(10):881. https://doi.org/10.3390/f10100881
18. Axelsson BOM, Grundberg SA, Grönlund JA (1991) The use of gray scale images when evaluating disturbances in cutting force due to changes in wood structure and tool shape. Eur J Wood Wood Prod 49(12):491–494. https://doi.org/10.1007/BF02619482
19. Axelsson BOM, Lundberg ÅS, Grönlund JA (1993) Studies of the main cutting force at and near a cutting edge. Eur J Wood Wood Prod 51(1):43–48. https://doi.org/10.1007/BF02615376
20. Axelsson B (1993) Cutting forces at a tool edge during machining of wood. Doctoral dissertation, Luleå tekniska universitet, Sweden
21. Lundberg S (1994) Experimental investigations in wood machining related to cutting forces, sawdust gluing, and surface roughness. Doctoral dissertation, Luleå tekniska universitet, Sweden
22 Chuchala D, Orlowski K, Sandak A, Sandak J, Pauliny D, Barański J (2014) The effect of wood provenance and density on cutting forces while sawing Scots pine (Pinus sylvestris L.). BioResources 9(3):5349–5361. https://doi.org/10.15376/biores.9.3.5349-5361
23. Chuchala D, Ochrymiuk T, Orlowski K, Lackowski M, Taube P (2020) Predicting cutting power for band sawing process of pine and beech wood dried with the use of four different methods.

BioResources 15(1):1844–1860. https://doi.org/10.15376/biores.15.1.1844-1860
24. Licow R, Chuchala D, Deja M, Orlowski K, Taube P (2020) Effect of pine impregnation and feed speed on sound level and cutting power in wood sawing. J Clean Prod 272:122833. https://doi.org/10.1016/j.jclepro.2020.122833
25. Sinn G, Chuchala D, Orlowski KA, Taube P (2020) Cutting model parameters from frame sawing of natural and impregnated Scots pine (*Pinus sylvestris* L.). Eur J Wood Wood Prod 78:777–784. https://doi.org/10.1007/s00107-020-01562-5
26 Chuchala D, Sandak A, Orlowski KA, Sandak J, Eggertsson O, Landowski M (2021) Characterization of Arctic driftwood as naturally modified material. Part 1: machinability. Coatings 11:278. https://doi.org/10.3390/coatings11030278
27. Caceres C, Uliana L, Hernández R (2018) Orthogonal cutting study of wood and knots of white spruce. Wood and Fiber Science 50(1):55–65. https://doi.org/10.22382/wfs-2018-006
28 Kivimaa E (1952) Die Schnittkraft in der Holzbearbeitung. (The cutting force in wood processing). Holz Roh- Werkst 10(3):94–108. https://doi.org/10.1007/BF02608840
29. Moradpour P, Doosthoseini K, Scholz F, Tarmian A (2013) Cutting forces in bandsaw processing of oak and beech wood as affected by wood moisture content and cutting directions. Eur J Wood Prod 71:747–754. https://doi.org/10.1007/s00107-013-0734-z
30 Pinkowski G, Krauss A, Sydor M (2016) The effect of spiral grain on energy requirement of plane milling of Scots pine (Pinus sylvestris L.) wood. BioResources 11(4):9302–9310. https://doi.org/10.15376/biores.11.4.9302-9310
31. Zhu Z, Buck D, Ekevad M, Marklund B, Guo X, Cao P, Zhu N (2019) Cutting forces and chip formation revisited based on orthogonal cutting of Scots pine. Holzforschung 73(2):131–138. https://doi.org/10.1515/hf-2018-0037
32. Curti R, Marcon B, Denaud L, Togni T, Furferi R, Goli G (2021) Generalized cutting force model for peripheral milling of wood, based on the effect of density, uncut chip cross section, grain orientation and tool helix angle. Eur J Wood Prod 79:667–678. https://doi.org/10.1007/s00107-021-01667-5
33. Cristóvão L, Broman O, Grönlund A, Ekevad M, Sitoe R (2012) Main cutting force models for two species of tropical wood. Wood Mat Sci Eng 7(3):143–149. https://doi.org/10.1080/17480272.2012.662996
34. Hernandez RE, Llave AM, Kouba A (2014) Effects of cutting parameters on cutting forces and surface quality of black spruce cants. Eur J Wood Wood Prod 72:107–116. https://doi.org/10.1007/s00107-013-0762-8
35. Zhu Z, Guo X, Ekevad M, Cao P, Na B, Zhu N (2017) The effects of cutting parameters and tool geometry on cutting forces and tool wear in milling high-density fiberboard with ceramic cutting tools. Int J Adv Manuf Technol 91:4033–4404. https://doi.org/10.1007/s00170-017-0085-8
36. Nasir V, Cool J (2018) A review on wood machining: characterization, optimization, and monitoring of the sawing process. Wood Mat Sci Eng 15(1):1–16. https://doi.org/10.1080/17480272.2018.1465465
37. Pantscharowitsch M, Kromoser B (2022) Influence of machining parameters on subtractive manufacturing of elementary geometries in glued-laminated timber using an industrial robot. Wood Mat Sci Eng 18(2):472–490. https://doi.org/10.1080/17480272.2022.2051734
38. Berglund A, Broman O, Grönlund A, Fredriksson M (2013) Improved log rotation using information from a computed tomography scanner. Comput Electron Agric 90:152–158. https://doi.org/10.1016/j.compag.2012.09.012
39. Fredriksson M (2012) Reconstruction of *Pinus Sylvestris* knots using measurable log features in the Swedish pine stem bank. Scand J For Res 27(5):481–491. https://doi.org/10.1080/02827581.2012.656142
40. Fredriksson M (2014) Log sawing position optimization using computed tomography scanning. Wood Mat Sci Eng 9(2):110–119. https://doi.org/10.1080/17480272.2014.904430
41. Fredriksson M (2015) Optimizing sawing of boards for furniture production using CT log scanning. J Wood Sci 61(5):474–480. https://doi.org/10.1007/s10086-015-1500-0
42. Meulenberg V, Ekevad M, Svensson M (2021) Thin kerf cutting forces of frozen and non-frozen Norway spruce and Scots pine wood. Wood Mat Sci Eng 16(6):414–420. https://doi.org/10.1080/17480272.2021.1925964
43. Meulenberg V, Ekevad M, Svensson M (2022) Minor cutting edge angles of sawing teeth: effect on cutting forces in wood. Eur J Wood Wood Prod 80(5):1165–1173. https://doi.org/10.1007/s00107-022-01833-3
44. Meulenberg V, Ekevad M, Svensson M, Broman O (2022) Minor cutting edge force contribution in wood bandsawing. J Wood Sci 68(1):18. https://doi.org/10.1186/s10086-022-02023-8
45. Sachs L (1984) Applied statistics. A handbook of techniques, 2nd edn. Springer, New York
46. Dinwoodie JM (2000) Timber. Its nature and behaviour. CRC Press, London, UK. https://doi.org/10.4324/9780203477878
47. Mikkola MT, Korhonen RK (2013) Effect of latewood proportion on mechanical properties of Finnish pine wood modified with compression drying. Wood Fiber Sci 45(4):335–342
48. Hansson L, Cherepanova E (2012) Determination of wood moisture properties using a CT-scanner in a controlled low-temperature environment. Wood Mat Sci Eng 7(2):87–92. https://doi.org/10.1080/17480272.2012.662701
49. Beaulieu J, Dutilleul P (2019) Applications of computed tomography (CT) scanning technology in forest research: a timely update and review. Can J For Res 49(10):1173–1188. https://doi.org/10.1139/cjfr-2018-0537
50. Seguy S, Arnaud L, Insperger T (2014) Chatter in interrupted turning with geometrical defects: an industrial case study. Int J Adv Manuf Technol 75:45–56. https://doi.org/10.1007/s00170-014-6120-0
51. Agic A (2018) Analysis of entry phase in intermittent machining. Licentiate Thesis Production Technology, University West, Sweden
52. Dvoracek O, Lechowicz D, Krenke T, Möseler B, Tippner J, Haas F, Emsenhuber G, Frybort S (2021) Development of a novel device for analysis of high-speed cutting processes considering the influence of dynamic factors. Int J Adv Manuf Technol 113:1685–1697. https://doi.org/10.1007/s00170-021-06769-1
53. Kubík P, Šebek F, Krejčí P, Brabec M, Tippner J, Dvořáček O, Lechowicz D, Frybort S (2023) Linear woodcutting of European beech: experiments and computations. Wood Sci Technol 57:51–74. https://doi.org/10.1007/s00226-022-01442-6

Part of the results and analysis presented in the above paper were presented at the 25th International Wood Machining Seminar, Portmesse Nagoya, Japan, 4–7 October 2023, and at Konstelacja Szkół Naukowych w Inżynierii Mechanicznej, Koszalin-Dźwirzyno, Poland, 16–18 October 2023.